# Se site targeted-two circles antioxidant in GPx4–like catalytic peroxide degradation by polyphenols (−)-epigallocatechin gallate and genistein using SERS

Mengmeng Zhang [a], Jingbo Liu [a], Yu Gao [b], Bing Zhao [c], Meng-Lei Xu [a,c,*], Ting Zhang [a,*]

[a] Jilin Provincial Key Laboratory of Nutrition and Functional Food/ College of Food Science and Engineering, Jilin University, Changchun 130062, PR China
[b] College of Plant Protection, Jilin Agricultural University, Changchun 130118, PR China
[c] State Key Laboratory of Supramolecular Structure and Materials, College of Chemistry, Jilin University, Changchun 130012, PR China

ABSTRACT

A Se site targeted-two circles antioxidant of polyphenols EGCG and genistein in glutathione peroxidase 4 (GPx4)–like catalytic peroxide $H_2O_2$ and cumene hydroperoxide degradation was demonstrated by surface-enhanced Raman scattering (SERS). Se atom's active center is presenting a 'low-oxidation' and a 'high-oxidation' catalytic cycle. The former is oxidized to selenenic acid (SeO$^-$) with a Raman bond at 619/ 610 cm$^{-1}$ assigned to the $\nu$O − Se by the hydroperoxide substrate at 544/ 551 cm$^{-1}$ assigned to $\omega$HSeC decreased. Under oxidative stress, the enzyme shifted to 'high-oxidation' catalytic cycle, in which GPx4 shuttles between R-SeO$^-$ and R-SeOO$^-$ with a Raman intensity of bond at 840/ 860 cm$^{-1}$ assigned to $\nu$O=Se. EGCG could act as a reducing agent both in $H_2O_2$ and Cu-OOH degradation, while, genistein can only reduce Cu-OOH, because it binds more readily to the selenium site in GPx4 than EGCG with a closer proximity, therefore may affect its simultaneous binding to coenzymes.

## 1. Introduction

Food-borne plant polyphenols are micronutrients present in plants as essential physiological compounds with biological activities, whose antioxidant function as inhibitors of reactive oxygen species (ROS) generation based on their chemical structure has attracted much attention (Pathiraja et al., 2023). The harm of oxidative stress lies in ROS can induce cellular damage since they can attack cellular membranes by reacting with polyunsaturated fatty acids and with sulfhydryl bonds present in some proteins, leading to the development of several diseases, such as neurodegenerative disease (Xu et al., 2016). Organisms counter oxidative stress by increasing the activity of antioxidant enzymes and the activation of related signalling pathways (Xie, Cai, Zhao, Li, & Tian, 2020). Polyphenols act on antioxidant enzymes through signalling pathways, or example, glutathione peroxidase (GPx), and actively alter antioxidant activities, thus acting as antagonists of oxidative stress (Cianciosi et al., 2022). Among GPxs, GPx1–4 and 6 (expressed in humans) are selenoproteins that contain selenocysteine in the enzyme active site, GPx4 plays a unique antioxidant enzyme that repairs oxidative damages induced in the cellular membranes playing a critical role in the cellular lipid oxidative stress dissipation (Forcina & Dixon, 2019).

The antioxidant properties of phenolic compounds are influenced by molecular structure, particularly the number and location of hydroxyl groups, and by the nature of substitutions on aromatic rings (Pereira, Valentão, Pereira, & Andrade, 2009). Phenolic compounds can be divided into several groups based on their structural characteristics. Among them, flavonoids, which contains the common C6–C3–C6 structure, are the largest group of polyphenols (Tsao, 2010). (−)-Epigallocatechin-3-gallate (EGCG), a catechin compound found abundantly in tea, while, genistein, one isoflavone of soybean with a C6–C2–C6 structure (Gao, Xu, Xu, Shi, & Xiong, 2020). While, due to the hydroxylation pattern and variations in the chromane ring, the former belongs to flavanol, the latter is belongs to isoflavone. As a result, the antioxidant potential of single compounds can differ due to their structure and location of hydroxyl groups (Xu et al., 2015). However, it remains unclear how flavonoid, such as EGCG or genistein, interacts with antioxidant enzymes and affects enzyme structure, especially the source of ROS

divided into organic peroxides and inorganic peroxide due to structural changes difficult to characterize.

The commonly used methods for studying protein structure include X-ray diffraction, nuclear magnetic resonance, and cryo electron microscopy, which reveal detailed information on protein folding and conformation. However, these methods are limited to purifying proteins, or requiring frozen fixed cells. There are problems such as insufficient sensitivity in analysis and inability to reflect changes in the structure of biological macromolecules under physiological conditions (Zhu et al., 2024). Surface-enhanced Raman scattering (SERS) is an ultra-sensitive and rapid vibrational spectroscopy technique that can investigate the structural and conformational information of molecules, including proteins, small molecules, and their interactions (Xu, Gao, Han, & Zhao, 2017) (Xu et al., 2020) (Xu, Gao, Han, & Zhao, 2022). The main advantage of SERS is that it could be used in recognition studies using bioactive compounds under physiological conditions. Further, it can characterize the interactions between adsorbates and rough metal substrate and the orientation of the molecule adsorbed on the surfaces (Zhao et al., 2022). Thus, SERS is an attractive analytical tool to investigate the spatial conformation of EGCG or genistein when it interacts with glutathione peroxidase (Xu, Zhao, & Ozaki, 2023).

Inspired by this, in the present study, spectral method, such as Raman, SERS, ultravioletvisible spectroscopy (UV − Vis), molecular docking and PC12 cell viability test were performed to determine molecular interactions between polyphenols EGCG or genistein and GPx4 and its reducing agent activity assay in GPx4 − like catalytic cycle, then reported ROS degradation with different sources. Selenium related Raman vibration modes in GPx − like catalytic cycle were also obtained. Overall, this study provides insight into the molecular mechanism between polyphenols and GPx4 and the innovative anti-oxidation mechanism of polyphenols.

## 2. Experimental

### 2.1. Chemicals

Recombinant GPx4 protein *mus musculus* (mouse) was obtained from Cloud−Clone Crop. (Wuhan, China). EGCG, genistein and selenium dioxide $SeO_2$ (IV) were purchased from Aladdin (Shanghai, China). $H_2O_2$ (30%), cumene hydroperoxide (Cu-OOH), sodium dihydrogen phosphate ($NaH_2PO_4$), disodium hydrogen phosphate ($Na_2HPO_4$), glutathione (GSH), glutathione reductase (GR), sodium citrate ($Na_3C_6H_5O_7$, 99.8%), dimethyl sulfoxide (DMSO) and silver nitrate ($AgNO_3$, 99.0%) were obtained from Sigma-Aldrich (Shanghai, China). MTS [3-(4,5-dimethylthiazol-2-yl)-5-(3-carboxymethoxyphenyl)-2-(4-sulfophenyl)-2H-tetrazolium, inner salt] was purchased from Promega (Madison, USA). Dulbecco's modified eagle medium (DMEM), fetal calf serum (FBS), penicillin–streptomycin, and phosphate-buffered saline (PBS) were obtained from Gibco (Grand Island, NY, USA). Cell-culture plates and cell-culture dishes were purchased from Corning Incorporated (USA). PC12 cells were provided by Shanghai Cellular Institute of China Scientific Academy. Structure of part chemicals as shown in Table A1. A total glutathione peroxidase assay kit with nicotinamide adenine dinucleotide phosphate (NADPH) was purchased from the Beyotime Institute of Biotechnology (Shanghai, China). The principle of testing is as follows:

$$2GSH + R - OOH \xrightarrow{GPx} GSSH + R - OH + H_2O$$

$$NADPH + H^+ + GSSH \xrightarrow{GR} NADP^+ + 2GSH$$
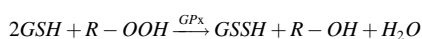
### 2.2. Apparatus

Raman and SERS spectrum were obtained using a confocal Raman spectrometer (LabRam ARAMIS, Yvon/HORIBA) with a 633 nm excitation from a HeNe laser. The laser beam with a power of 1.0 mW on the sample was used ona microscope with a magnification of $50\times$ objective lens. The silicon wafer (band at 520.7 $cm^{-1}$) was used to calibrate the spectrometer, and the measurement range was from 400 to 1800 $cm^{-1}$. The Raman spectrum was acquired from pure solid powder on a glass slide. The SERS spectrum was acquired using Ag nanoparticles (Ag NPs) described above. UV − Vis spectroscopy extinction spectra were measured with a Lambda1050+ spectrophotometer (Perkinelmer).

### 2.3. Synthesis of Ag NPs and preparation of selenious acid solution ($H_2SeO_3$)

#### 2.3.1. Synthesis of Ag NPs

Ag NPs were prepared according to the Lee and Meisel method (Lee & Meisel, 1982). Briefly, 36.00 mg $AgNO_3$ was added to 200 mL $H_2O$, and after 4 mL of trisodium citrate solution (1% ω/V) was added when the boil started. After heating for 40 min at 85 °C, a grey-green colloid mixture was formed, and the solution was cooled at room temperature (Xu et al., 2020).

#### 2.3.2. Preparation of $H_2SeO_3$

Selenious acid solution ($H_2SeO_3$) was prepared using $SeO_2$ and water. For that, 11.00 mg $SeO_2$ was added to 10.00 mL $H_2O$, then $100.00 \times 10^{-6}$ $mol·L^{-1}$ $H_2SeO_3$ were gained.

### 2.4. GPx4–like catalytic peroxide degradation by polyphenols

The reaction cycle of GPx4 was measured by the conventional test (Orian et al., 2015). Briefly, the activity assay was performed at various concentrations of $H_2O_2$ (ranging from 3 to 6 mM), Cu-OOH (ranging from 3 to 6 mM), GPx4 (ranging from 10 to 20 μg/mL), and EGCG/ genistein (ranging from 0.75 to 1.50 mM). After that, 0.20 mM NADPH and 0.50 IU/ml GR were added to the samples, and the volume was adjusted to the same buffer. Ag NPs was added as the same volume. Raman/ SERS spectra were obtained using a He─Ne laser (633 nm) with a laser power of 50 mW under 10 s exposure time and 10 times accumulation. UV − Vis spectroscopy extinction spectra were scanning from 200 nm to 1000 nm.

### 2.5. Cell culture and cell viability assay

PC12 cells were cultured on collagen-coated dishes in DMEM medium supplemented with 10% FBS, 100.00 U/mL penicillin, and 100.00 μg/mL streptomycin at 37 °C in a humidified atmosphere of 5% $CO_2$ incubator (Xu et al., 2016). Genistein was dissolved in DMSO (the concentration of DMSO in the final culture medium was <0.1%), and PC12 cells ($1 \times 10^5$ cells per mL) were seeded into a 96-well plate and grown in the incubator for 24 h, then exposed to genistein (10.00–40.00 μg/mL). The control group was treated with PBS. In protective experiments, PC12 cells were divided into five groups, Control check: After seeded 24 h, PC12 cells were treated with PBS. Positive group: After seeded 24 h, PC12 cells were treated with $H_2O_2$ or Cu-OOH (100.00 μg/mL). Pretreatment group: After seeded 12 h, PC12 cells were treated with genistein and incubated for 12 h, then treated with $H_2O_2$ (14 mmol) or Cu-OOH (300.00 μmol). Co-treatment group: After seeded 24 h, PC12 cells were treated with $H_2O_2$ (14 mmol) or Cu-OOH (300.00 μmol) and treated with genistein simultaneously. Post-treatment group: After seeded 24 h, PC12 cells were treated with $H_2O_2$ (14 mmol) or Cu-OOH (300.00 μmol) and incubated for 12 h, then treated with GEN, DAI, or the mixed solution. All treatments were incubated for 48 h. PC12 cells viability after various treatments were assessed by the MTS.

### 2.6. Theoretical calculation

The interaction effect between EGCG/ genistein and GPx4 was analysis by the AutoDock Vina program (version 1.1.2), after structure

optimized by applying DFT method using the Gaussian 09 program. Firstly, the 6–311++G(d,p) basis set was used for the H, C, O, and Se atoms, while the LanL2DZ basis set was used for the Ag atom. All calculations were performed using the Gaussian 09 software program. Then, the probable interaction between EGCG and GPx4 determined by the AutoDock Vina program. The high-resolution crystal structure of GPx4 (2.7 Å) was downloaded from the RCSB Protein Data Bank (http ://www.rcsb.org/pdb). The water molecules were removed from GPx4 before docking calculations. The AutoDock Tools was used to add polar hydrogen atoms into the GPx4 molecule. The structure of EGCG was obtained using ChemOffice 2010. Protein and ligand files in the PDBQT format were used as input for molecular docking. In Vina docking, the Grid box dimensions size was set to 126 Å in x × y × z directions with a grid spacing of 1 Å. Docking calculations were performed with the AutoDock Vina program (Lian et al., 2019). The figures were obtained from the PyMol software. The schematic diagrams of EGCG–GPx4 and genistein–GPx4 interactions for docking pose were generated using the LigPlus program.

### 2.7. Statistical analysis

The data analyzed by SPSS 16.0 were mean ± SD based on Duncan's Multiple Range (SSR) test at $p < 0.05$ level (*) and $p < 0.01$ level (**), respectively.

## 3. Results and discussions

### 3.1. Construction of GPx4–like catalytic peroxide degradation by EGCG

#### 3.1.1. GPx4–like catalytic $H_2O_2$ degradation by EGCG

GPx4 − like catalytic cycle peroxide degradation by EGCG was detected by using a standard GR-coupled GPx4 assay with a UV − Vis spectrophotometer, while, peroxide degradation by GSH was control group. Ag NPs with an absorption of around 430 nm were also added, and increased the maximum absorbance due to the localized surface plasmon resonance (Fig. S1A). EGCG could act as a reducing agent like GSH in $H_2O_2$ degradation as shown in Fig. S2B, a decrease of maximum absorbance around 220 nm was detected with the reduction of $H_2O_2$ in both EGCG and GSH with good linearity. Furthermore, a decrease at 330 nm was also detected, while a decrease at 340 nm was in Fig. S2A, indicating that NADPH was consumed. However, in the absence of NADPH, no GPx − like activity was observed for EGCG from 1 to 10 min (Fig. S3A).

To confirm that GPx4–like catalytic $H_2O_2$ was degraded in the reaction by EGCG, the product in the reaction mixture was analyzed by Raman and *in-situ* SERS spectra, as shown in Fig. S4 and Fig. 1. The signal−to−noise ratio of the Raman spectrum was significantly lower (Fig. S4).The SERS spectrum showed significant changes after $H_2O_2$ treatment with 633 nm laser wavelength is of high quality. Therefore, the results demonstrated that the 633 nm laser line is the optimal excitation wavelength for SERS measurements and quantitative analysis. Among them, the peak at 876 cm$^{-1}$ during the GPx4-like catalytic cycle of EGCG was assigned to O − O from $H_2O_2$ was observed once $H_2O_2$ was added compared to other spectra, which was similar to previous studies (Ebrahimi, Viell, Mitsos, Mhamdi, & Brandhorst, 2017; Ghosh, Prasad, & Mugesh, 2019; Molinari & Wachs, 2010). During the GPx-like catalytic cycle of EGCG was measured by *in-situ* SERS spectrum (ranging from 400 to 1800 cm$^{-1}$) and SERS bands were observed at 443, 762, 806, 876, 914, 1178, 1370, and 1620 cm$^{-1}$ (Fig. 1B). Additionally, the band at 876 cm$^{-1}$ assigned to stretching vibration of O − O ($vO − O$) from $H_2O_2$, and a decrease over time was observed (from 1 min to 10 min). No significant differences were observed in the SERS bands at 443, 1370, and 1620 cm$^{-1}$, however, bands at 762, 806, 914, and 1178 cm$^{-1}$ decreased over time ($p < 0.01$).

Generally speaking, the reducing agent in GPx catalytic is GSH, the results confirm the universal law of another GPx-like redox cycle, EGCG can also act as a reducing agent in $H_2O_2$ degradation. This was to say, EGCG acted as the substrates of GPx4, and NADPH acted as an indispensable co-enzyme. The reaction between $H_2O_2$ and the GPx4 could be the first step in the GPx4-like catalytic cycle, and the same result can be obtained using both reducing agents, EGCG or GSH. The GPx1 can promote the reduction of $H_2O_2$ by the active-site selenocysteine, GPx4 has the same effect (Kóňa & Fabian, 2011). The *in-situ* SERS spectrum indicate that the ordered structure of the main chain of GPx4 did not change, while damage was observed in the side chain, such as tryptophan (Trp) and tyrosine (Tyr), the main chain of GPx4 was not changed by EGCG after addition of 3 mM $H_2O_2$ (Torrie, 1973) (Paria et al., 2015) (Table A2).

#### 3.1.2. GPx4–like catalytic Cu-OOH degradation by EGCG

In addition to $H_2O_2$, Cu-OOH was also used in this activity assay to determine if there is selectivity in reducing $H_2O_2$. GPx requires the simultaneous use of $H_2O_2$ and GSH to reduce $H_2O_2$ to $H_2O$, thereby converting GSH to GSSG. A decrease in the absorbance of Cu-OOH (at 225 nm) was monitoring using a UV − Vis spectrophotometer, which demonstrated EGCG could reduce the organic peroxides (Fig. S5A). The
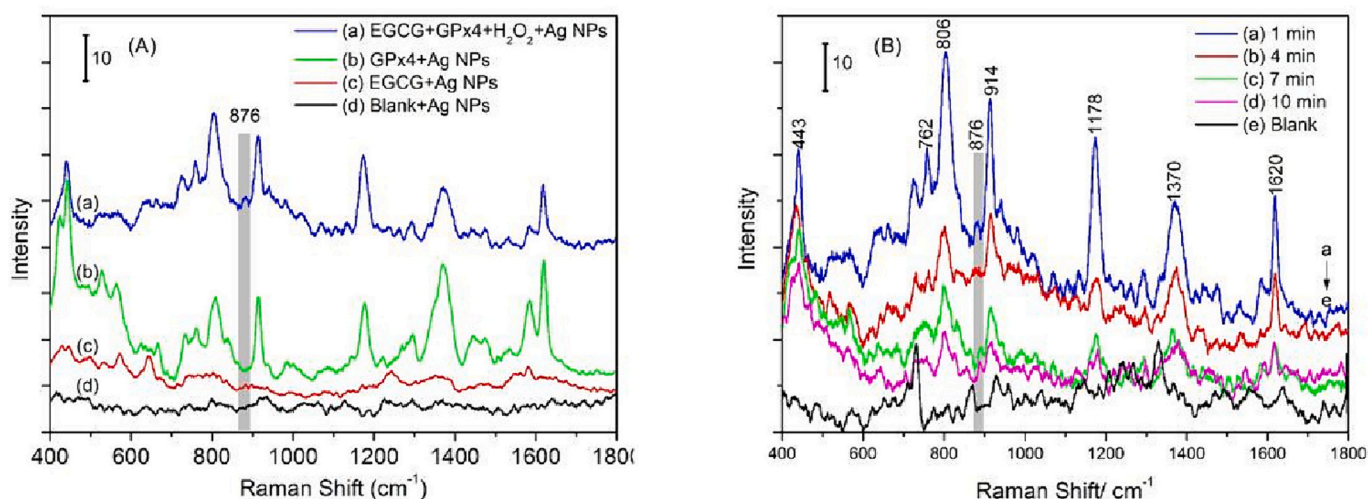


**Fig. 1.** SERS spectra and *in-situ* SERS spectra (400–1800 cm$^{-1}$) during GPx–like catalytic cycle of EGCG. A: (a) SERS spectra of EGCG after addition of 3 mM $H_2O_2$ at 1 min, (b) SERS spectra of GPx4 on Ag NPs, (c) SERS spectra of EGCG on Ag NPs. (d) Blank+Ag NPs; B: *In-situ* SERS spectra (400–1800 cm$^{-1}$) during GPx-like catalytic cycle of EGCG from 1 min to 10 min (a) 1 min, (b) 4 min, (c) 7 min, (d) 10 min, (e) blank.

Raman bond at 893 cm$^{-1}$ of ($\nu O - O$) also decreased from 1 min to 10 min, which is consistent with previous studies (Fig. S6) (Guo, Lee, Fukuzumi, & Nam, 2021; Paria et al., 2015). However, in the absence of NADPH and GR, no GPx-like activity was observed for EGCG, *i.e.*, no reduction of H$_2$O$_2$ (Fig. S3) or Cu-OOH occurred.

Both UV − Vis and SERS spectra demonstrated the capacity of EGCG to reduce peroxide, the mechanism of action of EGCG against oxidative stress *in vivo* is related to its antioxidant potential in the GPx4-like catalytic cycle. Furthermore, this antioxidant potential helps to maintain the normal redox status when cells are damaged by organic peroxide (Unno et al., 2021). In the GPx-like catalytic cycle, the NADPH can provide energy to maintain the reaction and act as an co-enzyme.

### 3.1.3. Effect of the concentration of individual substrates in GPx-like catalytic cycle by EGCG

To understand the concentration effect of some substrates on the reaction rate, the activity assay was performed using various concentrations of H$_2$O$_2$ (ranging from 3 to 6 mM), Cu-OOH (ranging from 3 to 6 mM), GPx4 (ranging from 10 to 20 μg/mL) and EGCG (ranging from 0.75 to 1.50 mM). The *in-situ* SERS spectra (400–1800 cm$^{-1}$) from 1 min to 10 min were shown in Fig. 2. When EGCG concentration decreased, the Raman intensity of H$_2$O$_2$ at 876 cm$^{-1}$ decreased from $39.13 \pm 3.70$ to $0.44 \pm 0.3$ after deducting the margin value. EGCG acts as a reducing agent and could promote the efficient removal of H$_2$O$_2$. Degradation efficiency declined as H$_2$O$_2$ concentration increased, or GPx4/EGCG concentration declined. When H$_2$O$_2$ concentration increased, the SERS bond at 876 cm$^{-1}$ decreased from $49.51 \pm 1.18$ to $2.74 \pm 4.32$ after deducting the margin value (Fig. 2B). Additionally, when GPx4 concentration decreased, the SERS bond at 876 cm$^{-1}$ decreased from $28.20 \pm 0.51$ to $23.83 \pm 3.33$ after deducting the background value (Fig. 2C). Noteworthy, EGCG concentration had a more important role in the early degradation reaction and this is possible to observe when line A and line B are compared in Fig. 2D. GPx4 enzyme activity determined the degradation rate of H$_2$O$_2$, as observed in Line C in Fig. 2D. The mechanism of the GPx-like catalytic cycle in Cu-OOH degradation was also evaluated. The SERS bonds at 893 cm$^{-1}$ are the characteristic peaks of Cu-OOH assigned to $\nu O - O$, and a decrease was observed with the Cu-OOH degradation. Therefore, it is possible to observe in Fig. 2E that when EGCG concentration decreased, the SERS bond at 893 cm$^{-1}$ also decreased from $17.33 \pm 1.02$ to $0.67 \pm 0.34$. When Cu-OOH concentration increased, the degradation efficiency was slower than in the

other two situations, from $46.10 \pm 0.83$ to $1.91 \pm 0.60$ (Fig. 2F). Notably, EGCG concentration had a more important role in the early degradation reaction, and EGCG had beneficial effects on cell membranes altered in diabetic conditions, by restoring transmembrane potential and by membrane 'stiffening' (Margina, Gradinaru, Manda, Neagoe, & Ilie, 2013).

### 3.2. Construction of GPx–like catalytic peroxide degradation by genistein

#### 3.2.1. GPx4–like catalytic peroxide degradation by genisten

Reducing agent activity of the genistein in the GPx4-like catalytic cycle assay was followed spectrophotometrically like which in EGCG. A decrease of maximum absorbance around 340 nm was detected with the reduction of Cu-OOH in genistein, however, no decrease detected of H$_2$O$_2$ in genistein (Fig. S6). Thus, genistein could act as a reducing agent like GSH in Cu-OOH degradation, however, it not worked in H$_2$O$_2$ degradation. SERS bands were observed at 443, 706, 809, 873, 913, 1177, 1371, 1584, and 1620 cm$^{-1}$. Among them, the peak at 873 cm$^{-1}$ during the GPx4-like catalytic cycle of genistein was assigned to O − O from Cu-OOH was observed once Cu-OOH was added compared to other spectra. 443, 706, 809, 913, 1177, 1371, 1584, and 1620 cm$^{-1}$ assigned to GPx4 (Fig. 3A). *In-situ* The SERS spectrum (ranging from 400 to 1800 cm$^{-1}$) during the GPx-like catalytic cycle of genistein was measured and, SERS bands at 873 cm$^{-1}$ assigned to O − O from Cu-OOH decrease with time. This is the same as the conclusion of UV spectrum. Thus, genistein could act as a reducing agent like GSH in Cu-OOH degradation when GPx4 and NADPH are present in the sample. No significant differences were observed in the SERS bands at 443 cm$^{-1}$, however, bands at 762, 806, 914, and 1178 cm$^{-1}$ decreased over time (Fig. 3B).

#### 3.2.2. Effect of the concentration of individual substrates in GPx-like catalytic cycle by genistein

Like EGCG, to understand the concentration effect of some substrates on the reaction rate, the activity assay was performed using various concentrations of Cu-OOH (ranging from 3 to 6 mM), GPx4 (ranging from 10 to 20 μg/mL) and genistein (ranging from 0.75 to 1.50 mM). The *in-situ* SERS spectra (400–1800 cm$^{-1}$) from 1 min to 10 min were shown in Fig. 4. In Fig. 4A, when genistein concentration decreased, the Raman intensity of Cu-OOH at 873 cm$^{-1}$ decreased from $13.52 \pm 0.33$ to $8.27 \pm 0.65$ after deducting the margin value. Genistein acts as a



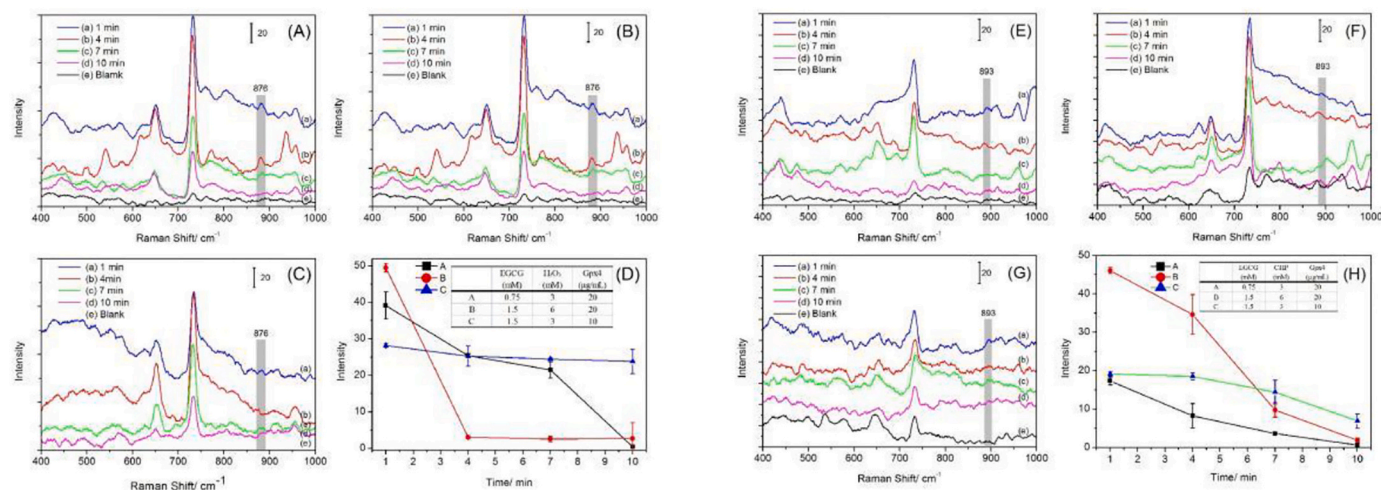**Fig. 2.** *In-situ* SERS spectra (400–1800 cm$^{-1}$) during GPx-like catalytic cycle of EGCG at various concentrations of EGCG (0.75–1.5 mM), H$_2$O$_2$ (3–6 mM), and GPx4 (10–20 μg/mL) at 1, 4, 7 and 10 min. **(A)** 0.75 mM EGCG+3 mM H$_2$O$_2$+ 20 μg/mL GPx4, **(B)** 1.5 mM EGCG+6 mM H$_2$O$_2$+ 20 μg/mL GPx4, **(C)** 1.5 mM EGCG+3 mM H$_2$O$_2$+ 10 μg/mL GPx4, **(D)** Intensity of SERS bond at 876 cm$^{-1}$. *In-situ* SERS spectra (400–1800 cm$^{-1}$) during GPx-like catalytic cycle of EGCG at various concentrations of EGCG (0.75–1.5 mM), Cu-OOH (3–6 mM), and GPx4 (10–20 μg/mL) at 1, 4, 7 and 10 min. **(E)** 0.75 mM EGCG+3 mM Cu-OOH+ 20 μg/mL GPx4, **(F)** 1.5 mM EGCG+6 mM Cu-OOH+ 20 μg/mL GPx4, **(G)** 1.5 mM EGCG+3 mM Cu-OOH+ 10 μg/mL GPx4, **(H)** Intensity of SERS bond at 893 cm$^{-1}$.

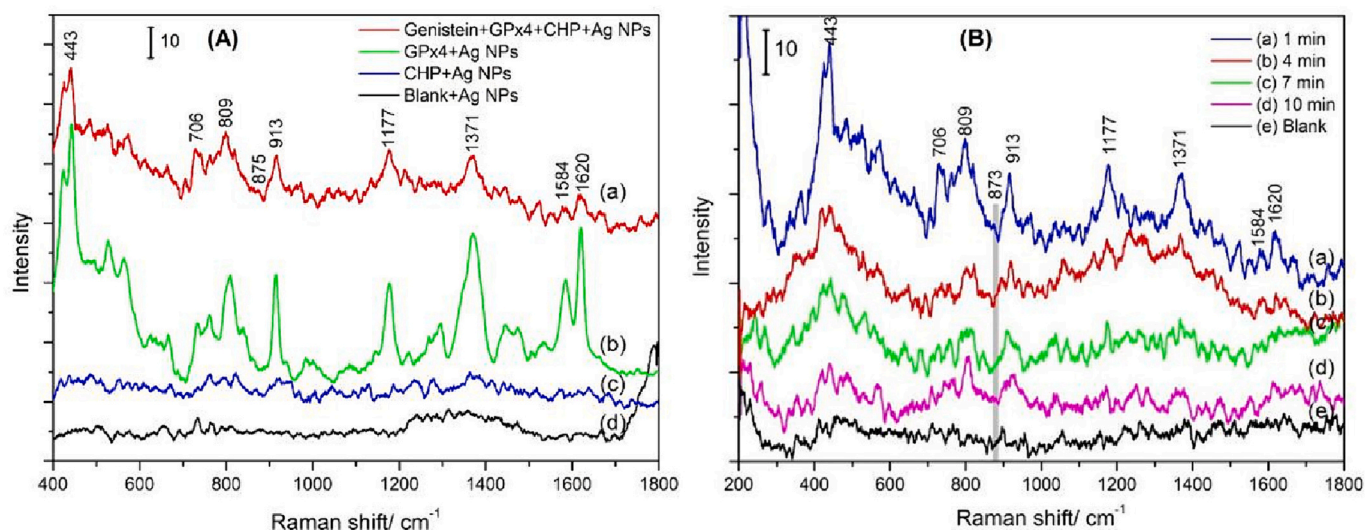**Fig. 3.** SERS spectra and *in-situ* SERS spectra (400–1800 cm$^{-1}$) during GPx–like catalytic cycle of genistein. **A:** SERS spectra (400–1800 cm$^{-1}$) during GPx–like catalytic cycle of genistein. (a) SERS spectra of genistein after addition of 3 mM cumene hydroperoxide (Cu-OOH) at 1 min, (b) SERS spectra of GPx4 on Ag NPs, (c) SERS spectra of Cu-OOH on Ag NPs. (d) Blank+Ag NPs. **B:** *in-situ* SERS spectra during GPx-like catalytic cycle of genistein from 1 min to 10 min. (a) 1 min, (b) 4 min, (c) 7 min, (d) 10 min.
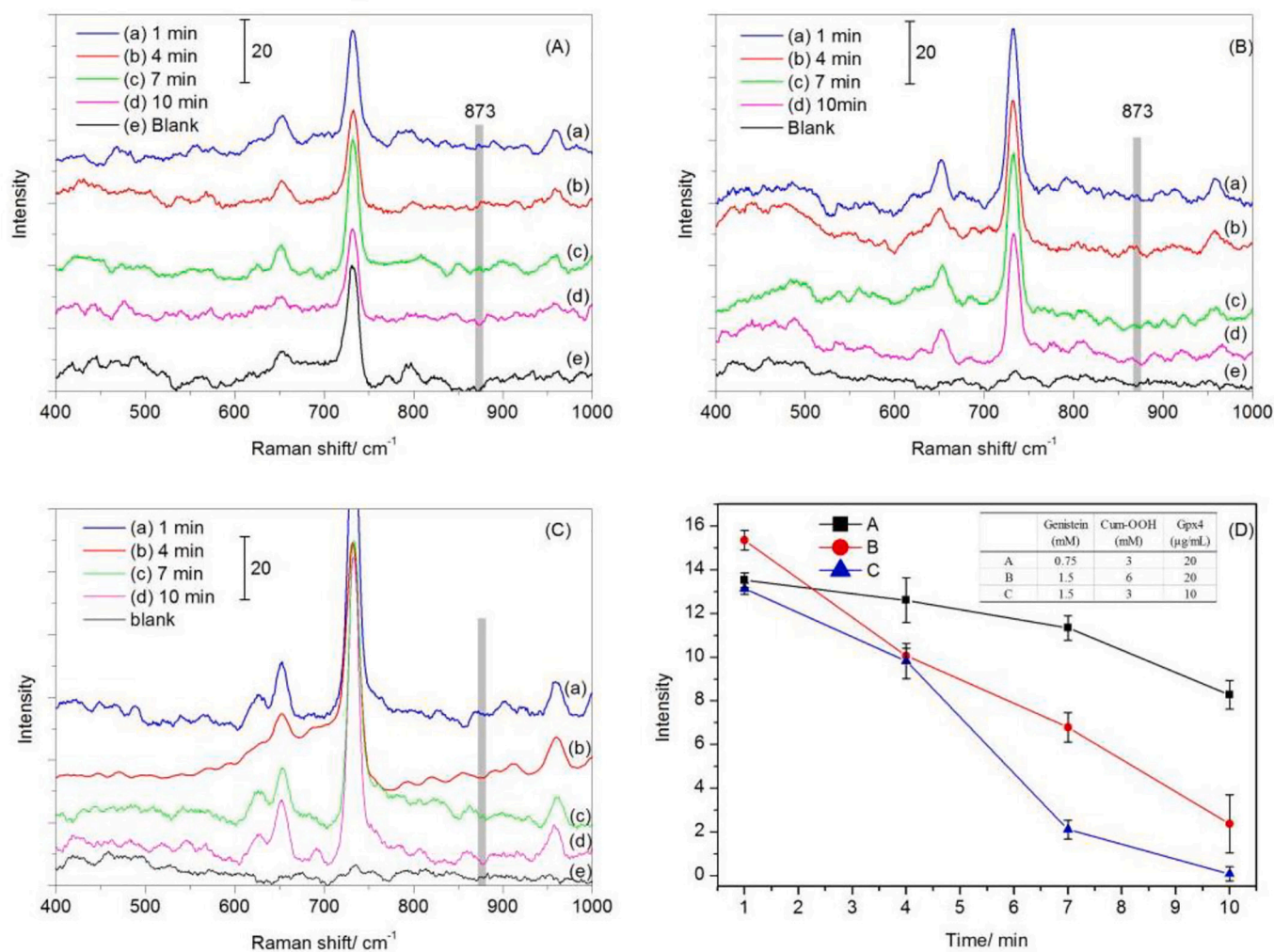


**Fig. 4.** *In-situ* SERS spectra (400–1800 cm$^{-1}$) during GPx-like catalytic cycle of genistein at various concentrations of genistein (0.75–1.5 mM), Cu-OOH (3–6 mM), and GPx4 (10–20 μg/mL) at 1, 4, 7 and 10 min. (A) 0.75 mM genistein+3 mM Cu-OOH+ 20 μg/mL GPx4, (B) 1.5 mM genistein+6 mM Cu-OOH+ 20 μg/mL GPx4, (C) 1.5 mM genistein+3 mM Cu-OOH+ 10 μg/mL GPx4, (D) Intensity of SERS bond at 873 cm$^{-1}$.

reducing agent and could promote the efficient removal of Cu-OOH, not for $H_2O_2$. Degradation efficiency increased as GPx4/genistein concentration increased. When $H_2O_2$ concentration increased, the SERS bond at 873 $cm^{-1}$ decreased from $15.35 \pm 0.45$ to $10.06 \pm 0.33$ after deducting the margin value (Fig. 4B). Additionally, when GPx4 concentration decreased, the SERS bond at 873 $cm^{-1}$ decreased from $13.13 \pm 0.26$ to $0.07 \pm 0.33$ after deducting the background value (Fig. 4C). Noteworthy, genistein concentration had a more important role in the early degradation reaction and this is possible to observe when line A and line B are compared in Fig. 4D. GPx4 enzyme activity determined the degradation rate of Cu-OOH, as observed in Line C in Fig. 4D.

### 3.2.3. Peroxide degradation by EGCG and genistein

Comparison between EGCG and genistein, EGCG could act as a reducing agent like GSH both in $H_2O_2$ and Cu-OOH degradation, while, genistein could worked in Cu-OOH degradation, not worked in $H_2O_2$ degradation. Concentration had a more important role in the early degradation reaction, GPx4 enzyme activity determined the degradation rate. In the absence of NADPH, no GPx − like activity was observed for EGCG or genistein. Thus, the different structures or hydroxyl groups determine their different antioxidant properties.

### 3.3. Mechanism of catalyst regeneration cycle

#### 3.3.1. DFT calculations of selenocysteine−SeOOH, selenocysteine−SeOH, and selenocysteine−SeH

Selenocysteine and its −SeOH and − SeOOH derivatives were geometry−optimized, and the theoretical Raman spectra of these three compounds at the B3LYP/6–311++G(d, p) level of theory are presented in Fig. S7. The absence of imaginary frequencies in the DFT calculations indicates that the calculated selenocysteine−SeH, selenocysteine−SeOH, and selenocysteine-SeOOH structures are minima on their respective potential energy surfaces. The calculated Raman vibrational modes in the frequencies ranging from 400 to 4000 $cm^{-1}$ are listed in Table A3. The Raman bands of selenocysteine at 538, 426, 671, and 913 $cm^{-1}$ can be assigned to $\delta O5C3C1 + \nu C10Se13$, $\omega HSe13C10$, $\rho HSe13C10$, and $\delta HSe13C10$, respectively. The Raman bands of selenocysteine at 538 and 601 $cm^{-1}$ can be assigned to $\nu C10Se13$ and $\nu O14Se13$, respectively. In selenocysteine−SeOOH, the Raman vibrational bands at 534, 577, 863, and 1118 $cm^{-1}$ can be assigned to $\omega HO5 + \nu C10Se$, $\nu O13Se$, $\nu O16Se$, and $\omega HO13Se$, respectively (Fig. S8). The results obtained in this study are similar to the theoretical Raman spectrum.

#### 3.3.2. Selenium related Raman vibration modes in GPx-like catalytic cycle

The Se atom is the active center of GPx4, and the valence changes the redox state to assign the bonds of Se–bond. The normal Raman and SERS spectra of $H_2SeO_3$ on Ag NPs are shown in Fig. S8. Among them, 443, 709, and 783 $cm^{-1}$ can be assigned to $\nu C − Se$, $\nu Se − O$, and $\nu Se{=}O$, respectively (Sanders, Louie, & Anderson, 2000).

#### 3.3.3. The reaction between peroxide and GPx4

As shown in Fig. 5A, the Raman intensity of the bond at 544 $cm^{-1}$ assigned to $\omega HSeC$ decreased after adding a concentration of $H_2O_2$ higher than 15 mM. This result showed that H—Se was oxidized. The Raman band was at 551 $cm^{-1}$ in Fig. 5B. The Raman band at 619 $cm^{-1}$ assigned to $\nu O − Se$ appeared when $H_2O_2$ concentration increased and reached the concentration of 15 mM. While, this Raman band at 610 $cm^{-1}$ assigned to $\nu O − Se$ appeared when Cu − OOH concentration increased in Fig. 5B. The Raman bond at 840 $cm^{-1}$ assigned to $\nu Se{=}O$ emerged when the concentration of $H_2O_2$ was increased to 25 mM, and this Raman band was at 860 $cm^{-1}$ in Fig. 5B with the same trends.

When the concentration is increased to 25 mM the oxidation of Se–OH to R − SeOO$^-$ occurs. The reaction of *peroxide* and GPx4 are the first steps in the GPx–like catalytic cycle. The catalytic mechanism of the GPx4 reaction involves redox shuttling of the Sec between the selenol (Se—H) and selenenic acid (Se–OH). Based on the observations from extensive *in situ* spectroscopic studies, this study can propose a plausible mechanism for EGCG or genistein and their GPx-like activity. In the resting ground state of the enzyme, the Sec is present as selenol (Se$^-$), which is oxidized to selenenic acid (SeO$^-$) by the hydroperoxide substrate as a 'low-oxidation' catalytic cycle (1st elementary reaction). Under oxidative stress, the enzyme might be shifted into the 'high-oxidation' catalytic cycle, in which the enzyme shuttles between R − SeO$^-$ and R − SeOO$^-$ (Borchert et al., 2018).

The former is oxidized to selenenic acid (SeO$^-$) with a Raman bond at 619 or 610 $cm^{-1}$ assigned to the $\nu O − Se$ by the hydroperoxide substrate at 544 or 551 $cm^{-1}$ assigned to $\omega HSeC$ decreased. Under oxidative stress, the enzyme shifted to 'high-oxidation' catalytic cycle, in which GPx4 shuttles between R − SeO$^-$ and R − SeOO$^-$ with a Raman intensity of bond at 840 or 860 $cm^{-1}$ assigned to $\nu O{=}Se$.

### 3.4. GPx-like catalytic cycle by genistein in PC12 cells

$H_2O_2$ (14 mmol) or Cu-OOH (300.00 μmol) for 24 h led to (61.51 ± 3.33)% and (43.40 ± 3.44)% viability. Genistein showed no protective effects in PC12 cells with $H_2O_2$ or Cu-OOH treatment ($p < 0.05$), however the Levene's test in homogeneity of variance test between Cu-OOH treatment and co-treatment with 40 μg/mL group showed the P is
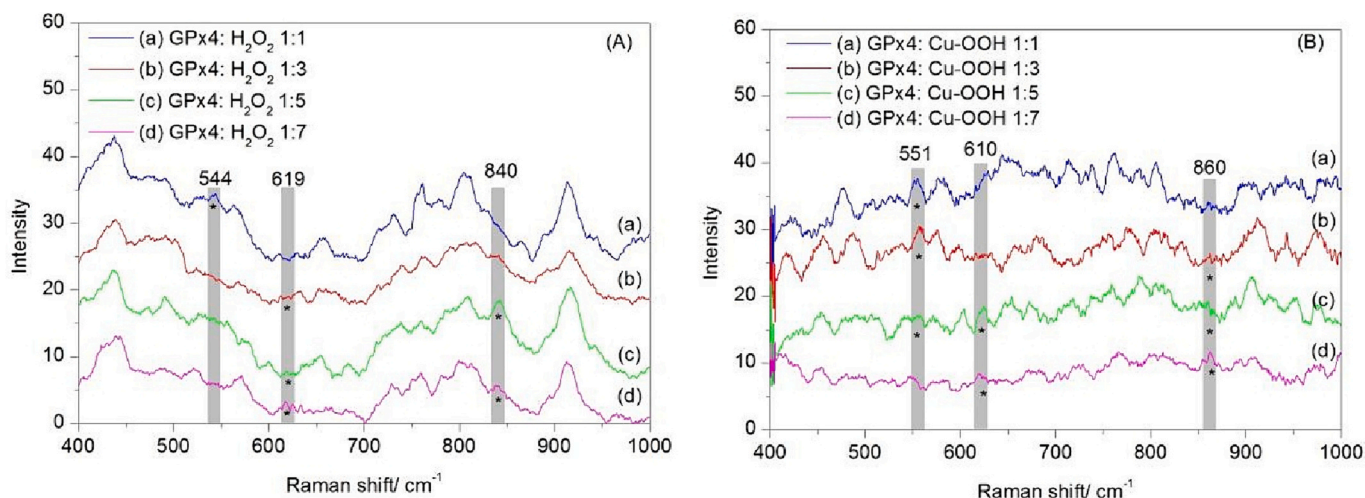


**Fig. 5.** Interaction between $H_2O_2$ (A), Cu-OOH (B) and GPx4 in different concentration ratios.

$1.9984 \times 10^{-15}$ much lower than 0.05, which means the difference in variance is statistically significant (Fig. 6).

### 3.5. Mechanism of GPx-like catalytic cycle by polyphenols by molecular docking

#### 3.5.1. Mechanism of GPx-like catalytic cycle by EGCG by molecular docking

Molecular docking is an essential tool to characterize the binding site of a drug with the protein. Furthermore, it could also be exploited to substantiate experimental observations (Li, Jiang, Pu, Cao, & Jiang, 2019). The docking conformation of the EGCG–GPx4 complex with the minimum binding energy was performed and presented in Fig. 7A. EGCG is docked into GPx4, and the binding energy was $-3.78$ kcal·mol$^{-1}$. The EGCG molecule was surrounded by 6 amino acid residues and interacting residues, including Gly–47, Lys–48, Met–156, Pro–155, Trp–136, and Cys with Se–746. Hydrogen bonds were observed between EGCG and Cys amino acid residues in CEase with a distance of 2.226 Å. These results were confirmed by Raman and SERS analyses. Previous studies have reported that the catalytic site of GPx4 is the Cys catalytic triad, and EGCG could interact with the Se–746 site in CEase *via* hydrogen bonding. The GPx4 lacks a surface-exposed loop domain, explaining the broad substrate specificity of GPx4 (Scheerer et al., 2007). The catalytic Cys oxidized to sufinic/sulfonic acid in the Cys mutein of GPx4, when the enzymes were oxidized in the absence of EGCG. The experimental outcome complied with molecular docking predictions, EGCG could act as a Se site targeted reducing agent in peroxide degradation with the GPx4–like catalytic cycle.

#### 3.5.2. Mechanism of GPx-like catalytic cycle by genistein by molecular docking

For genistein, the docking conformation of the genistein–GPx4 complex with the minimum binding energy as $-6.32$ kcal·mol$^{-1}$, however, the genistein was not located within the active pocket when they interacted under the lowest energy. While, in one of these interactions, genistein was located within the active pocket when they interacted with a binding energy as $-5.39$ kcal·mol$^{-1}$, which was lower than of EGCG as shown in Fig. 7B. The genistein molecule was surrounded by 5 amino acid residues and interacting residues, including Se–746, Lys–48, Met–156, Lys–135, and with Trp–136. Compared to EGCG–GPx4, geistein could interact with the Se–746 site in CEase, and Lys–48 *via* two hydrogen bonding with a distance of 1.966, 1.644 Å, respectively. The experimental outcome complied with molecular docking predictions.

#### 3.5.3. Structures determine different antioxidant properties of EGCG or genistein

Genistein could act as a Se site targeted reducing agent in peroxide degradation with the GPx4–like catalytic cycle. Although the
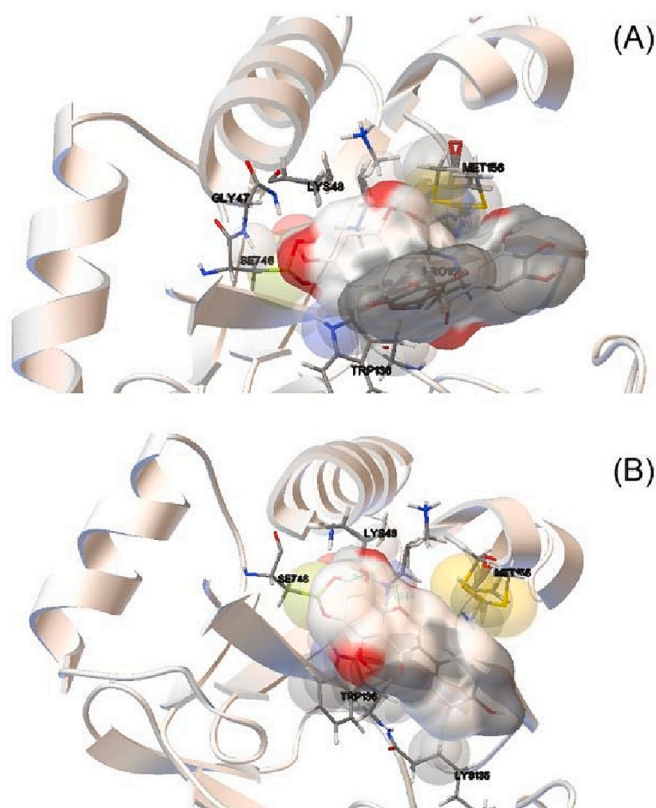


**Fig. 7.** The neighboring amino acids within a distance of 4 Å approximately EGCG (A), genistein (B) (the hydrogen bond between EGCG/genistein and GPx4 is shown as green dots at Se). (For interpretation of the references to colour in this figure legend, the reader is referred to the web version of this article.)

conformation bound to the selenium site is not the lowest energy, the binding is very tight. It is worth noting that, NADPH in this action acts as a coenzyme, thus, NADPH should also binding to GPx4 with different site against EGCG and genistein. Genistein binds more readily to the selenium site in GPx4 than EGCG with a closer proximity, and therefore may affect its simultaneous binding to coenzymes (Szelényi et al., 2019). This may be the reason why it can only reduce organic peroxides. This also explains that although it is not the lowest binding energy, it can show a good reduction effect in the experiment.

### 4. Conclusion

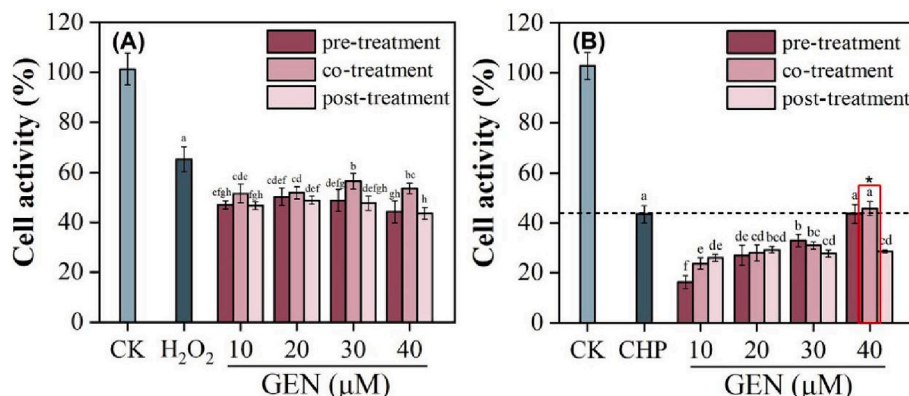This study demonstrated that the EGCG and genistein could act as a



**Fig. 6.** Genistein ameliorates in PC12 cell activity oxidative stress after $H_2O_2$ (A) or Cu-OOH treatment (B).

selenium site targeted reducing agent in peroxide degradation in the GPx4–like catalytic cycle with GPx4 and co-enzyme NADPH. The reaction of peroxide with the GPx4 is the first step in the GPx4 − like catalytic cycle, the ordered structure of the GPx4 main chain did not change, while, the side chain damage is obvious, such as Trp and Tyr. EGCG concentration had a more important role in the early degradation reaction, GPx4 enzyme activity determined the degradation rate. The Se atom active center and side-chain changed over time in the resting ground state of the enzyme. The *sec* is present as selenol (Se$^-$), which is oxidized to selenenic acid (SeO$^-$) by the hydroperoxide substrate as a 'low-oxidation' catalytic cycle. The catalytic site of GPx4 was the Cys catalytic triad, and EGCG or genistein could interact with the site of Se–746 *via* hydrogen bonding. Two cycles are likely to differ in this model depending on peroxide concentration. Genistein binds more readily to the selenium site in GPx4 than EGCG with a closer proximity, and therefore may affect its simultaneous binding to coenzymes. This study broadens the understanding of the antioxidant activity mechanism of polyphenols.

## CRediT authorship contribution statement

**Mengmeng Zhang:** Writing – original draft, Investigation. **Jingbo Liu:** Writing – review & editing. **Yu Gao:** Writing – review & editing. **Bing Zhao:** Writing – review & editing, Investigation. **Meng-Lei Xu:** Project administration, Investigation, Funding. **Ting Zhang:** Writing – review & editing.

## Declaration of competing interest

The authors declare no competing financial interest. The manuscript was written through contributions of all authors.

## Data availability

Data will be made available on request.

## Acknowledgments

## Appendix A. Supplementary data

Supplementary data to this article can be found online at https://doi.org/10.1016/j.fochx.2024.101387.

## References

Borchert, A., Kalms, J., Roth, S. R., Rademacher, M., Schmidt, A., Holzhutter, H.-G., Kuhn, H., & Scheerer, P. (2018). Crystal structure and functional characterization of selenocysteine-containing glutathione peroxidase 4 suggests an alternative mechanism of peroxide reduction. *Biochimica et Biophysica Acta (BBA) - Molecular and Cell Biology of Lipids, 1863*(9), 1095–1107. https://doi.org/10.1016/j.bbalip.2018.06.006

Cianciosi, D., Forbes-Hernández, T. Y., Regolo, L., Alvarez-Suarez, J. M., Navarro-Hortal, M. D., Xiao, J., Quiles, J. L., Battino, M., & Giampieri, F. (2022). The reciprocal interaction between polyphenols and other dietary compounds: Impact on bioavailability, antioxidant capacity and other physico-chemical and nutritional parameters. *Food Chemistry, 375*, 131904. https://doi.org/10.1016/j.foodchem.2021.131904

Ebrahimi, F., Viell, J., Mitsos, A., Mhamdi, A., & Brandhorst, M. (2017). In-line monitoring of hydrogen peroxide in two-phase reactions using raman spectroscopy. *AICHE Journal, 63*(9), 3994–4002. https://doi.org/10.1002/aic.15754

Forcina, G. C., & Dixon, S. J. (2019). GPX4 at the crossroads of lipid homeostasis and Ferroptosis. *PROTEOMICS, 19*(18), 1800311. https://doi.org/10.1002/pmic.201800311

Gao, Y., Xu, J., Xu, M., Shi, S., & Xiong, J. (2020). Genistein and daidzein reduced chlorpyrifos induced damage in PC12 cell. *Oil Crop Science, 5*(1), 1–5. https://doi.org/10.1016/j.ocsci.2020.03.008

Ghosh, S., Prasad, S., & Mugesh, G. (2019). Understanding the role of oxo and peroxido species in the glutathione peroxidase (GPx)-like activity of metal based nanozymes. *Inorganica Chimica Acta, 484*, 283–290. https://doi.org/10.1016/j.ica.2018.09.045

Guo, M., Lee, Y.-M., Fukuzumi, S., & Nam, W. (2021). Biomimetic metal-oxidant adducts as active oxidants in oxidation reactions. *Coordination Chemistry Reviews, 435*, Article 213807. https://doi.org/10.1016/j.ccr.2021.213807

Kóňa, J., & Fabian, W. M. F. (2011). Hybrid QM/MM calculations on the first redox step of the catalytic cycle of bovine glutathione peroxidase GPX1. *Journal of Chemical Theory and Computation, 7*(8), 2610–2616. https://doi.org/10.1021/ct200129q

Lee, P. C., & Meisel, D. C. (1982). Adsorption and surface-enhanced Raman of dyes on silver and gold sols. *The Journal of Physical Chemistry, 86*, 3391–3395.

Li, X., Jiang, H., Pu, Y., Cao, J., & Jiang, W. (2019). Inhibitory effect of condensed tannins from banana pulp on cholesterol esterase and mechanisms of interaction. *Journal of Agricultural and Food Chemistry, 67*(51), 14066–14073. https://doi.org/10.1021/acs.jafc.9b05212

Lian, W., Liu, Y., Yang, H., Ma, H., Su, R., Han, X., Zhao, B., & Niu, L. (2019). Investigation of the binding sites and orientation of Norfloxacin on bovine serum albumin by surface enhanced Raman scattering and molecular docking. *Spectrochimica Acta Part A: Molecular and Biomolecular Spectroscopy, 207*, 307–312. https://doi.org/10.1016/j.saa.2018.09.034

Margina, D., Gradinaru, D., Manda, G., Neagoe, I., & Ilie, M. (2013). Membranar effects exerted in vitro by polyphenols – Quercetin, epigallocatechin gallate and curcumin – On HUVEC and Jurkat cells, relevant for diabetes mellitus. *Food and Chemical Toxicology, 61*, 86–93. https://doi.org/10.1016/j.fct.2013.02.046

Molinari, J. E., & Wachs, I. E. (2010). Presence of surface vanadium peroxo-oxo umbrella structures in supported vanadium oxide catalysts: Fact or fiction? *Journal of the American Chemical Society, 132*(36), 12559–12561. https://doi.org/10.1021/ja105392g

Orian, L., Mauri, P., Roveri, A., Toppo, S., Benazzi, L., Bosello-Travain, V., Palma, A. D., Maiorino, M., Miotto, G., Zaccarin, M., Polimeno, A., Flohe, L., & Ursini, F. (2015). Selenocysteine oxidation in glutathione peroxidase catalysis: An MS-supported quantum mechanics study. *Free Radical Biology and Medicine, 87*, 1–14. https://doi.org/10.1016/j.freeradbiomed.2015.06.011

Paria, S., Ohta, T., Morimoto, Y., Ogura, T., Sugimoto, H., Fujieda, N., Goto, K., Asano, K., Suzuki, T., & Itoh, S. (2015). Generation, characterization, and reactivity of a CuII–Alkylperoxide/anilino radical complex: Insight into the O–O bond cleavage mechanism. *Journal of the American Chemical Society, 137*(34), 10870–10873. https://doi.org/10.1021/jacs.5b04104

Pathiraja, D., Wanasundara, J. P. D., Elessawy, F. M., Purves, R. W., Vandenberg, A., & Shand, P. J. (2023). Water-soluble phenolic compounds and their putative antioxidant activities in the seed coats from different lentil (Lens culinaris) genotypes. *Food Chemistry, 407*, Article 135145. https://doi.org/10.1016/j.foodchem.2022.135145

Pereira, D. M., Valentão, P., Pereira, J. A., & Andrade, P. B. (2009). Phenolics: from chemistry to biology. *Molecules, 14*, 2202–2211.

Sanders, A., Louie, M., & Anderson, A. (2000). Raman spectra of selenious acid at low temperatures. *Journal of Raman Spectroscopy, 31*(12), 1057–1060. https://doi.org/10.1002/1097-4555(200012)31:12<1057::AID-JRS643>3.0.CO;2-2

Scheerer, P., Borchert, A., Krauss, N., Wessner, H., Gerth, C., Höhne, W., & Kuhn, H. (2007). Structural basis for catalytic activity and enzyme polymerization of phospholipid hydroperoxide glutathione peroxidase-4 (GPx4). *Biochemistry, 46*(31), 9041–9049. https://doi.org/10.1021/bi700840d

Szelényi, P., Somogyi, A., Sarnyai, F., Zámbó, V., Simon-Szabó, L., Kereszturi, É., & Csala, M. (2019). Microsomal pre-receptor cortisol production is inhibited by resveratrol and epigallocatechin gallate through different mechanisms. *BioFactors, 45*(2), 236–243. https://doi.org/10.1002/biof.1477

Torrie, B. H. (1973). Raman and infrared spectra of Na2SeO3, NaHSeO3, H2SeO3, and NaH3(SeO3)2. *Canadian Journal of Physics, 51*(6), 610–615. https://doi.org/10.1139/p73-080

Tsao, R. (2010). Chemistry and biochemistry of dietary polyphenols. *Nutrients, 2*, 1231–1246.

Unno, T., Araki, Y., Inagaki, S., Kobayashi, M., Ichitani, M., Takihara, T., & Kinugasa, H. (2021). Fructooligosaccharides increase in plasma concentration of (−)-Epigallocatechin-3-Gallate in rats. *Journal of Agricultural and Food Chemistry, 69*(49), 14849–14855. https://doi.org/10.1021/acs.jafc.1c05991

Xie, L.-W., Cai, S., Zhao, T.-S., Li, M., & Tian, Y. (2020). Green tea derivative (−)-epigallocatechin-3-gallate (EGCG) confers protection against ionizing radiation-induced intestinal epithelial cell death both in vitro and in vivo. *Free Radical Biology and Medicine, 161*, 175–186. https://doi.org/10.1016/j.freeradbiomed.2020.10.012

Xu, M.-L., Gao, Y., Han, X. X., & Zhao, B. (2017). Detection of pesticide residues in food using surface-enhanced Raman spectroscopy: A review. *Journal of Agricultural and Food Chemistry, 65*(32), 6719–6726. https://doi.org/10.1021/acs.jafc.7b02504

Xu, M.-L., Gao, Y., Han, X.-X., & Zhao, B. (2022). Innovative application of SERS in food quality and safety: A brief review of recent trends. *Foods, 11*.

Xu, M.-L., Gao, Y., Jin, J., Xiong, J.-F., Han, X. X., & Zhao, B. (2020). Role of 2–13C isotopic glyphosate adsorption on silver nanoparticles based on ninhydrin reaction: A study based on surface—Enhanced Raman spectroscopy. *Nanomaterials, 10*.

Xu, M.-L., Gao, Y., Wang, X., Xiong, J., Chen, X., Zhao, S., Ma, S., Huang, Y., & Liu, J. (2016). Effect of carbaryl on some biochemical changes in PC12 cells: The protective effect of soy isoflavone genistein, and daidzein, and their mixed solution. *CyTA Journal of Food, 14*(4), 587–593. https://doi.org/10.1080/19476337.2016.1181107

Xu, M.-L., Liu, J., Zhu, C., Gao, Y., Zhao, S., Liu, W., & Zhang, Y. (2015). Interactions between soy isoflavones and other bioactive compounds: A review of their

potentially beneficial health effects. *Phytochemistry Reviews, 14*(3), 459–467. https://doi.org/10.1007/s11101-015-9398-0

Xu, M.-L., Zhao, B., & Ozaki, Y. (2023). Surface-enhanced Raman scattering (SERS) sensors for food safety. *Encyclopedia of Sensors and Biosensors, 4,* 456–470.

Zhao, J., Wang, J., Liu, Y., Han, X. X., Xu, B., Ozaki, Y., & Zhao, B. (2022). Detection of prostate cancer biomarkers via a SERS-based aptasensor. *Biosensors and Bioelectronics, 216*, Article 114660. https://doi.org/10.1016/j.bios.2022.114660

Zhu, J., Zhu, J., Xie, H., Tang, J., Miao, Y., Cai, L., Hildebrandt, P., & Han, X. X. (2024). In situ Raman spectroscopy reveals cytochrome c redox-controlled modulation of mitochondrial membrane permeabilization that triggers apoptosis. *Nano Letters, 24*(1), 370–377. https://doi.org/10.1021/acs.nanolett.3c04129